RESEARCH ARTICLE | JULY 01 2025

Coaxial barrier discharge in argon flow excited by pulse groups of periodic voltage: Plasma structures formation in the discharge zone and plasma jet

Yu. Akishev ; S. Ermolaeva ; M. Medvedev ; A. Petryakov ; K. Hajisharifi ; H. Mehdian ; E. Robert

Phys. Plasmas 32, 073501 (2025)
https://doi.org/10.1063/5.0272401

Coaxial barrier discharge in argon flow excited by pulse groups of periodic voltage: Plasma structures formation in the discharge zone and plasma jet

Cite as: Phys. Plasmas **32**, 073501 (2025); doi: 10.1063/5.0272401
Submitted: 24 March 2025 · Accepted: 9 June 2025 ·
Published Online: 1 July 2025

Yu. Akishev,[1,2,3,a] S. Ermolaeva,[3] M. Medvedev,[1,3] A. Petryakov,[1] K. Hajisharifi,[4] H. Mehdian,[4] and E. Robert[5]

AFFILIATIONS

[1]State Research Center of Russian Federation Troitsk Institute for Innovative and Fusion Research, Pushkovikh Str. 12, Troitsk, Moscow 108840, Russia
[2]National Research Nuclear University MEPHI, Kashirskoe shosse 31, Moscow 115409, Russia
[3]The Gamaleya National Center of Epidemiology and Microbiology, Gamaleya Str. 18, Moscow 123098, Russia
[4]Plasma Medicine Group, Faculty of Physics, Kharazmi University, Tehran 15719-14911, Iran
[5]UMR 7344 GREMI, CNRS/Université d'Orléans, Orléans, France

[a)]**Author to whom correspondence should be addressed:** akishev@triniti.ru

ABSTRACT

The subject of this study is a coaxial barrier discharge in an argon flow at atmospheric pressure. The discharge was excited by short pulses of sinusoidal voltage, the repetition frequency of which varied. This article presents the results of experimental studies on the dynamics of plasma structures created inside a discharge tube and in a plasma jet. The influence of the previous pulse group on the discharge and plasma jet structures in the subsequent pulse group was established by varying the repetition frequency of the pulse groups. It was found that at a low repetition frequency, streamers in the jet have a snake shape, and at a high frequency, streamers propagate in the jet in a straight line along its axis. Using high-speed and multi-frame imaging of the discharge, the formation of diffuse and constricted plasma structures inside the discharge zone and in plasma jet has been established. It is shown that the diffuse and constricted plasma structures inside a discharge tube, in fact, are the surface ionization waves identical to both the ionization waves propagating inside long capillary tube and along flat dielectric barrier in a surface barrier discharge.

I. INTRODUCTION

Barrier discharge in dielectric tubes purged with inert gas (He, Ar) or its mixture with molecular gas (N_2, O_2, H_2O, etc.) is widely used to create low-temperature plasma jets propagating in air at atmospheric pressure.[1–4] Such jets contain a large number of biochemically and physically reactive particles, such as metastables, radicals, charged particles, etc. For this reason, cold plasma jets are successfully used for the surface treatment of thermally unstable materials, including living tissues.[5–9] When choosing a plasma-forming gas, its price also matters for practice. Therefore, in many cases, argon may be preferable, since it is significantly cheaper than helium.

The effectiveness of plasma treatment of targets significantly depends on the composition and concentration of reactive particles delivered by the plasma jet to the treated surface.[10–13] In turn, the composition and concentration of reactive particles entering the target are determined by composition of the plasma-forming gas. If speak shortly, the primary reactive species are generated in the discharge zone exclusively from the plasma-forming gas. Furthermore, they are blown by a flow of plasma-forming gas into the ambient air. The latter mixes with the plasma jet containing primary reactive particles. The presence of humid air drastically changes the set of plasma-chemical processes, which provide fast transformation of the primary reactive species into secondary ones (some of them can be even unwanted, for instance, ozone) eventually entering the target. Thus, the main processes responsible for the reactive species composition in the discharge zone and plasma jet are essentially different. Therefore, it is reasonably to distinguish two stages in the dynamics of reactive particles formation.

The first stage is associated with the reactive particles generation in the discharge zone bounded by dielectric walls insulating the plasma-forming gas from ambient air. The second stage is associated with the plasma-chemical transformation of the primary reactive particles in the course of their transfer by a plasma jet from the discharge zone up to the target surface. In this case, ambient air molecules diffusing into the plasma jet are involved in the processes of plasma-chemical transformation as well. It is clear that the second stage essentially influences the plasma-chemical efficiency of the gas-discharge devices. On the other hand, gas-discharge and gasdynamic processes in the first stage have a significant impact on the plasma-chemical processes in the second stage. Therefore, in order to select optimal plasma jet regimes, it is necessary to know the properties of both stages; in particular, it is necessary to know the shape of their plasma structures, within which the birth and transformation of reactive particles take place. A reason is that the diffuse and constricted plasma structures differ significantly in current density in them. This leads to the fact that the intensity of the reactive particle generation is different in the zone of diffuse and constricted plasma. In addition, the ratio between the volumes occupied by diffuse and constricted plasma also is important. Therefore, knowledge of the actual shape of plasma structures is essential matter for determining the efficiency of reactive particle generation.

Plasma generators with a thin rod electrode, which is located coaxially inside a dielectric tube, are widely used to create cold plasma jets. A grounded electrode in the form of a wide metal strip is wrapped around the outside of the tube,[14,15] or the metal body of the plasma source plays the role of a grounded electrode.[5,8] There are designs in which the thin electrode either is completely inside the zone bounded by the grounded electrode or does not enter this zone, being located upstream. A high pulsed, pulse-periodic or sinusoidal voltage is applied to the thin electrode. This plasma source design has certain technical advantages. However, the gas discharge zone is fully closed in it and inaccessible for monitoring the dynamics of the discharge spatial structure. For this reason, most of the known experimental information on the study of the properties of such sources relates to the characterization only of the radial and longitudinal structures of the plasma jet in isolation from the discharge structure that gave rise to it. With that said, the elucidation of the coaxial barrier discharge structure inside the tube and its effect on the plasma jet structure is of both scientific and practical interest.

Argon, compared to helium, is an easily ionizable gas. In addition, metastable atoms can rapidly accumulate in the discharge with argon. Metastables make a significant contribution to the charged particles balance due to stepwise ionization.[16,17] In addition, argon is almost 10 times more massive than helium, so the diffusion smoothing of the plasma and gaseous inhomogeneities in the argon plasma is slower. For this reason, ionization instability, which leads to the discharge constriction, that is, to the thin current filament formation, develops faster in argon and at lower energy deposits compared to discharge in helium. In this case, the structure of both the barrier discharge in the argon-purged tube and the argon plasma jet may differ markedly from similar structures of the barrier discharge in helium.

Currently, there are two points of view on this issue. It was shown in Refs. 18–20 that the structure of an argon plasma jet created by an MW discharge is formed by straight-line propagating streamers, also called ionization waves of bullet-type. At the same time, it was shown in Ref. 21 that ionization waves inside a gas-discharge tube with argon look like curved snake-type streamers. In fact, the authors investigated the development of two counter ionization waves generated in a long capillary tube by a pulsed periodic barrier discharge. Moreover, from the data presented in Ref. 21, it is impossible to draw an unambiguous conclusion about whether curved streamers are surface or bulk ionization waves. It should also be noted that a plasma jet was not created in experiments.[21] Therefore, strictly speaking, the results of Ref. 21 cannot be attributed to the study of the ionization waves structure in argon plasma jets.

In this paper, for the first time, the dynamics of plasma structures of a coaxial barrier discharge in an argon flow is studied in detail both inside the discharge zone and in a plasma jet outside the discharge zone. The discharge was excited by short pulse-periodic groups ("zugs" in German, this term is used through the text) of sinusoidal voltage. The succession frequency of zugs has been varied. Such mode of excitation made it possible to establish a scenario for the plasma structures development in the discharge and plasma jet from the very first half-cycle in the zug as well as to identify the influence of the previous zug on the plasma structures development in the subsequent zug, depending on the zug's frequency. Using high-speed and multi-frame imaging of the discharge, the presence of diffuse and constricted plasma inside the discharge zone and in plasma jet is shown, and the dynamics of their structure is investigated. By shooting the discharge in two perpendicular directions, it was established that the diffuse and constricted plasma in the discharge zone, in fact, are the surface ionization waves. It is concluded that they are identical to the ionization waves propagating inside long capillary tubes[22–24] as well as along the flat surface of dielectrics in a surface barrier discharge.[25]

II. EXPERIMENTAL SETUP

The experiments were carried out with a coaxial barrier discharge, forming a plasma jet exiting into a free space with atmospheric air [Fig. 1(a)]. The barrier discharge was ignited in a thin-walled capillary quartz tube 2 with an inner/outer diameter of 2.5/4.0 mm, respectively, and a length of 60 mm. The dielectric constant of quartz is $\varepsilon = 3.76$ at 20 °C and a frequency of 1 MHz. A high-voltage electrode 1 made of a thin tungsten wire with a diameter of 0.3 mm was placed inside the tube along its axis. A thin copper foil 3 with a width of 20 mm was glued to the outer side surface of the dielectric tube. This foil served as a grounded electrode. A 2 mm wide slit was cut in the foil along the tube to monitor the discharge image. Figure 1(b) shows the waveform of a single zug of sinusoidal voltage with the frequency of 125 kHz. The voltage amplitude in the zug decreases over time for about 10 periods.

A Redline Technologies G2000 generator was used as a source of high-voltage sinusoidal voltage, which created sinusoidal voltage zugs with a frequency of 125 kHz and decreasing amplitude [Fig. 1(b)]. The generator provided a smooth adjustment of the amplitude of the first half-cycle and zug's frequency in the range of 0.5–5 kV and 100 Hz–20 kHz, respectively. Electrical signals (currents and voltages) were recorded with good temporal resolution. Barrier discharge voltage was measured by an ACTAKOM ACA-6039 voltage probe with a 220 MHz bandwidth and a measuring range of 0–40 kV. The electrical signals were recorded by a Rhode&Schwartz RTE1204 4-channel digital oscilloscope with a bandwidth of 2 GHz.

Gaseous argon with an argon content of 99.9999% by volume was used in the experiments. The argon flow rate through the

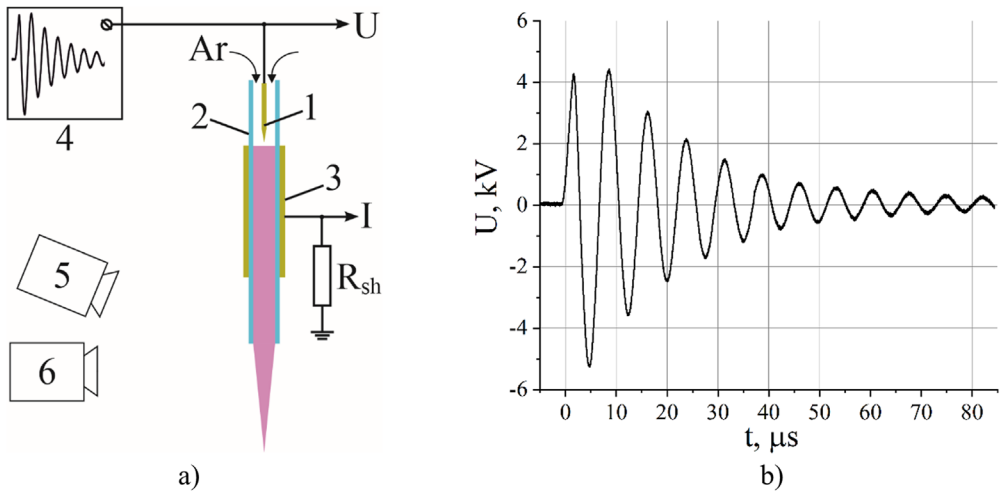

FIG. 1. (a) Sketch of the discharge tube section, optical devices, and electrical circuits. Current shunt resistance $R_{sh} = 50\ \Omega$. 1 and 3—high voltage and grounded electrodes; 2—quartz tube; 4—high-voltage sinusoidal generator Redline G2000, 5—photo camera Canon EOS 5D, 6—sCMOS-camera PCO DICAM C4. (b) The waveform of a single zug.

discharge tube was 7.5 ± 0.1 slm and measured with RMS-0.63 rotameter (argon measuring range up to 9.6 slm, and error is 0.1 slm). The jet velocity at the quartz tube outlet and along the jet was measured using a Pitot tube coupled with a Testo-510 differential pressure gauge (measuring range up to 100 hPa, and error is $\pm$ 0.05 hPa). At a given argon flow rate, the Reynolds number was about three times the critical value for smooth pipes $Re* \approx 2200–2300$, and, therefore, the gas flow inside the used capillary tube was turbulent. After exiting the tube into the ambient air, the jet becomes even more turbulent, as a result of which its velocity and temperature decrease quite quickly as it moves away from the tube outlet. The gas temperature at different points of the jet and around the jet was measured with a chromel-alumel thermocouple (type K) with a measuring range from -40 to $+230\,^{\circ}$C and a measurement accuracy of 1%–3% (UT70A device). The discharge was captured with a Canon EOS 5D camera (20 Megapixel resolution, exposure time of 125 μs or more) as well as an ICCD camera sCMOS-camera PCO DICAM C4 (four frames with a maximum resolution of 2048×2048 and exposure of 51 ns, and the time shift between frames varies from 1 ns to several milliseconds).

The experimental setup as a whole was used for implementation of all experiments. In the experiments, the pause τ between neighbor zugs was the subject to changing. The selected values of τ satisfied two conditions: $\tau > t_r$ and $\tau < t_r$, where $t_r = \frac{l}{V}$, l is the length of the discharge zone, and V is the gas flow velocity inside the tube. Thus, time t_r is the characteristic residence time of gas inside the tube. At atmospheric pressure, plasma is "freezing" into neutral gas and moves jointly with it. Therefore, the value t_r is also the plasma residence time in the tube. In our experiments, the time t_r is equal about 1 ms. The first condition $\tau > t_r$ corresponds to that the plasma created in the previous zug is completely removed from the discharge zone by the time the next zug appears. In other words, the condition $\tau > t_r$ means that the plasma of the previous zug has no effect on the discharge development in the next zug. In such a case, studying the discharge development in a single zug gives the information about the establishment stage of a stationary sinusoidal discharge as well.

The converse condition $\tau < t_r$ means a strong influence of the previous zug on the next one. It is clear that the situation for discharge development in zugs will be much different under conditions $\tau > t_r$ and $\tau < t_r$. Therefore, the presentation of the experimental material is divided into two parts. The first part presents the results obtained when the condition $\tau > t_r$ is fulfilled. The second part contains experimental data for the condition $\tau < t_r$. In each part, only the first three or four half-periods of the zug are considered in detail because in the remaining half-periods, everything repeats. The obtained results are presented in Part I and Part II of Sec. III.

III. RESULTS OF THE EXPERIMENTS

A. Part I ($\tau > t_r$): The zug repetition frequency $F = 100$ Hz, $\tau = 10$ ms

Every zug of damped sinusoidal voltage with a cyclic frequency of $f = 125$ kHz begins with a positive half-cycle, at the leading edge of which the first breakdown occurs inside the dielectric tube. The active phase with breakdowns in the discharge zone lasts 45 μs, after which the discharge stops. The characteristic waveforms of the discharge voltage and current as well as the energy deposited in the discharge during the entire zug are shown in Fig. 2.

Under the condition $\tau > t_r$, in the discharge zone, there is practically no plasma formed by the previous zug. Therefore, there is no noticeable number of seed electrons near the high-voltage electrode, which are necessary to initiate the first breakdown in the first half-cycle. Because of a shortage of seed electrons, there is a statistical scatter in the voltage of the first breakdown. In our experiment, this scatter ranges from $U_b \approx 1.7$ kV up to an amplitude voltage of $U_0 \approx 4.1$ kV. However, the breakdown voltage shows a different behavior for all subsequent half-periods. The fact is that the active phase duration in the zug is much shorter than the time needed for plasma removal from the discharge zone. Therefore, a discharge in the active phase is similar to a barrier discharge in a rest gas. In such a discharge, the plasma in the tube and the surface charge on the tube wall created in the previous half-cycle do not have time to completely disappear by the beginning

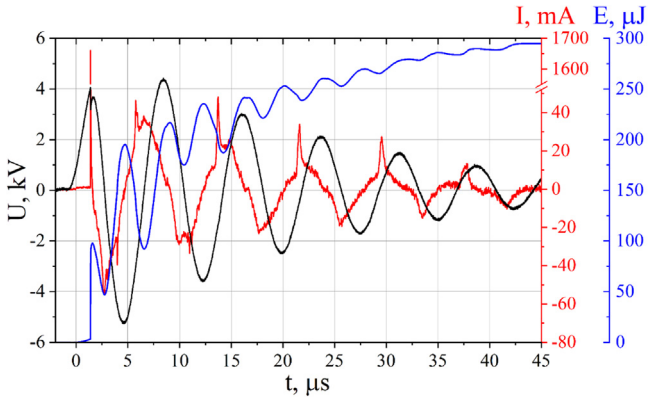

FIG. 2. The discharge voltage and current waveforms as well as the energy deposited in the discharge during the entire zug, at the voltage of the first breakdown $U_b = 4.1$ kV, $F = 100$ Hz.

of the next half-cycle. It means that they contribute essentially to reducing the breakdown voltage in this half-cycle. For this reason, the breakdown voltage and its scatter for all half-cycles of the zug, starting from the second, are significantly lower compared to their values in the first half-period.

1. Discharge structure dynamics in the first positive period for the stage ∂U/∂t > 0

The detailed discharge voltage and current waveforms corresponding to the first half-cycle and two different first breakdown voltages are shown in Fig. 3. One can see, the greater the breakdown voltage magnitude and the steeper the leading edge of the breakdown current, the greater its amplitude and the faster the decline on the trailing edge. As a rule, after a sharp decrease in the breakdown current, a quasi-stationary stage with a duration of about 1 μs and a current of several tens of mA is observed. As it turned out, strong breakdowns at $U_b \approx (4 \pm 0.1)$ kV occurred about 10 times more often than weak breakdowns at $U_b \approx (1.7 \pm 0.1)$ kV. For this reason, the main attention in the research was paid to the discharge development after strong breakdowns happening at $U_b \approx (4 \pm 0.1)$ kV.

The discharge current and voltage waveforms are complemented with discharge images obtained by using a fast 4-frame ICCD camera. The discharge images are synchronized with the current and voltage waveforms. Figure 4 shows in close-up two clippings from the current waveform presented in Fig. 3(b). The clippings correspond to the time of the first breakdown [Fig. 4(a)] and far after it [Fig. 4(b)]. In Fig. 4, a short-term small voltage drop at the moment of a current splash caused by a breakdown is associated with the influence of an external circuit. Green vertical lines in Fig. 4 mark the time points at which the discharge images in Fig. 5 were taken. Note, in these images and others through the paper, the blue color is a quartz tube, and the yellow color is the inner and outer electrodes.

As can be seen in Fig. 5, the breakdown takes place from the high-voltage electrode onto the inner surface of the quartz tube. After that, the developing plasma structure gradually fills the entire tube and exits, forming a plasma jet. At that, the developing plasma structure successively acquires different forms in each of the three zones of the barrier discharge (discharge zone, zone in the tube outside the discharge, and zone outside the tube).

First, the diffuse surface ionization wave adjacent to the tube inner surface appears in the vicinity of the high-voltage electrode and propagates further to the discharge zone exit. Note an existence of the slit in the outside electrode slightly disturbs azimuthal uniformity of the diffuse surface wave [see Fig. 5(c) with the rupture of the outer electrode]. Nevertheless, later through the text, we will refer to this tubular structure as an azimuthally uniform diffuse surface wave.

When an almost azimuthally homogeneous surface ionization wave reaches the discharge zone exit, it initiates here a current spot formation. After that, a thin current filament (surface streamer) originates from this spot and begins to elongate toward the tube exit. This streamer moves along the inner surface of the dielectric tube in a twisty snake-like trajectory. At the tube exit, the surface streamer turns into a volume streamer, which spreads inside the gas jet also along a winding trajectory. The diameters of the surface and volume streamer are

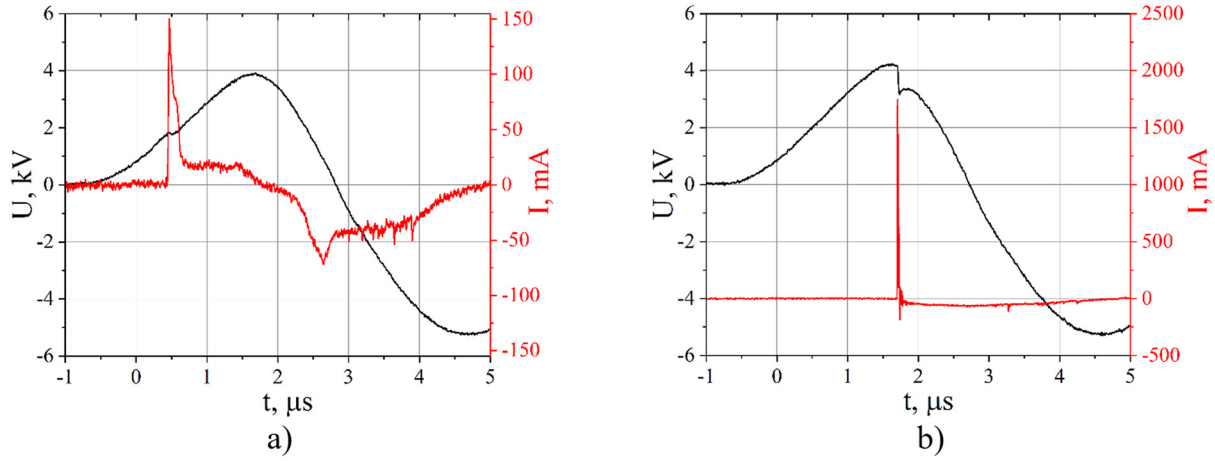

FIG. 3. The discharge voltage and current waveforms with the sharp breakdown current splashes in the first positive half-cycle of the zug. Breakdown voltage $U_b = 1.7$ (a) and 4.1 kV (b).

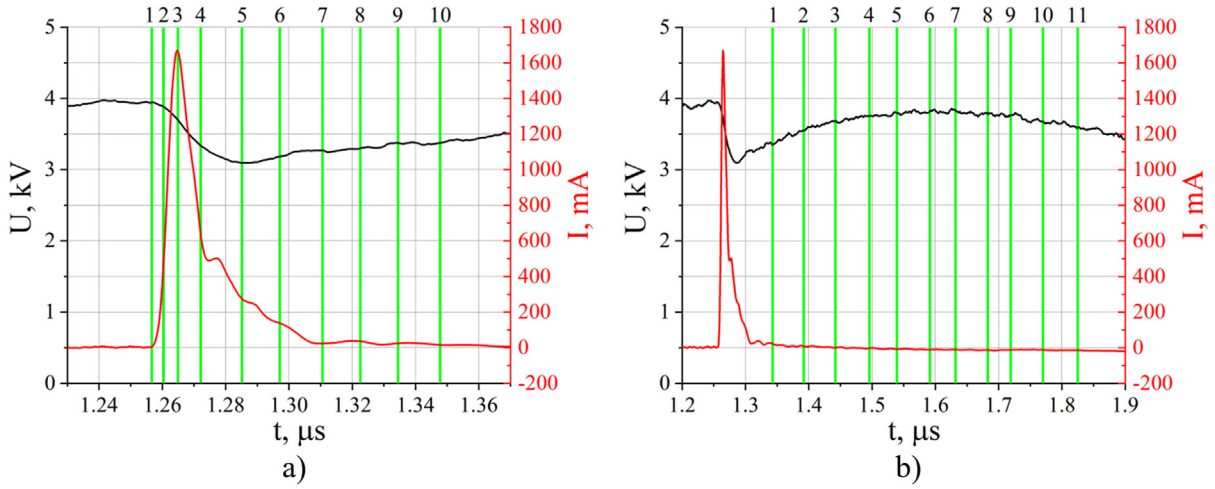

FIG. 4. Voltage and discharge current waveforms at the time around the first breakdown (a) and far later after it (b). The label numbers in (a) and (b) correspond to the frame numbers in Figs. 5(a) and 5(b). The vertical green lines mark position on the time axis of the frames shown in Figs. 5(a)–5(c). Breakdown voltage $U_b = 4$ kV.

approximately equal to each other but much smaller than the tube inner diameter. The volume streamer length depends on the magnitude of the first breakdown voltage; therefore, the lower the voltage breakdown, the shorter the volume streamer.

Eventually, after reducing the applied voltage, all these structures are destroyed. It is interesting that the volume streamer in the gas jet does not disappear simultaneously along its entire length. The streamer disappearance starts from its "tail," which moves in backward direction, that is, toward the tube exit. The plasma remaining after recombination of the constricted structures will be a source of seed electrons for the breakdown initiation in the next half-cycle. The surface charge deposited on the tube wall by the surface ionization wave will also contribute to the next breakdown.

The spatial distribution of ionization waves velocity is shown in Fig. 6. The velocities were calculated using the images shown in Fig. 5. An azimuthally uniform surface ionization wave propagating in the discharge zone has a maximum velocity (up to 10^8 cm/s) among other waves. After its transformation at the discharge zone exit into a surface streamer, the speed of the latter slows down sharply toward the tube outlet. At this place, the surface streamer transforms into a volume streamer, the velocity of which is non-monotonic along the jet. Its maximum velocity (about 7×10^6 cm/s) is reached at a distance from the tube equal to about 1/3 of the streamer length.

2. The discharge structure at the stage $\partial U/\partial t > 0$ starting from the first negative period

After the first breakdown, the applied voltage drops and reverses (see Fig. 2). This process is accompanied by disintegration of the plasma structure created before. Then, in the first negative half-cycle at the stage of the voltage growth ($\partial U/\partial t > 0$), a new breakdown occurs. The corresponding current and voltage waveforms, and discharge images are shown in Figs. 7 and 8. The vertical green lines in Fig. 7 show the position on the time axis of the frames given in Fig. 8.

In Fig. 8, the plasma structure evolution is shown for three characteristic time intervals: 1) during the breakdown (frames 1–7), 2) after the breakdown (frames 8–14), and 3) during the volume streamer decaying in the jet (frames 15–20). As can be seen, breakdown in this half-cycle occurs in the presence of a faintly luminous diffuse plasma in the discharge zone left over from the previous half-cycle. This is why the current spike associated with the breakdown at the tip of a needle is weakly expressed, although the simultaneous formation of a surface streamer and a tubular ionization wave occurs just at this moment. As a result, a complex plasma structure is formed (Fig. 8, frames 2–7), which expands in direction to the discharge zone exit (forward wave). In the course of movement, the plasma structure becomes layered—something like oblique ring-shaped strata can be observed (Fig. 8, frames 6–8).

When the leading edge of this structure approaches the discharge zone exit, a local current maximum occurs. At this moment (Fig. 8, frame 7), a bifurcation happens—the leading edge of this structure transforms into a surface streamer moving toward the tube outlet (Fig. 8, frames 9–10), and the trailing edge with a layered structure moves toward the high-voltage tip (backward wave, Fig. 8, frames 8–11). In the course of this movement, the layered structure of the backward surface ionization wave gradually disappears.

The formation of a volume streamer entering the plasma jet is initiated by the surface streamer when it arrives to the tube outlet (Fig. 8, frame 10). At the same time, the tubular diffuse plasma still remains in the tube. Next, the volume streamer in the plasma jet elongates along a curved trajectory (Fig. 8, frames 10–15). The streamer elongation stops with the beginning of the discharge current diminishing. At this stage, the decay of both the plasma inside the tube and the volume streamer in the plasma jet happens (Fig. 8, frames 16–20). Note that only a brightly glowing volume streamer is visible in the plasma jet. A reason is that the faintly glowing diffuse plasma around the bright volume streamer is not visible with a short exposure time of 100 ns.

The surface ionization waves velocity distribution in and outside the tube is shown in Fig. 9. The coordinates ($0 \le x \le 2$), ($2 \le x \le 3$), and ($x > 3$) correlate with the discharge zone, the tube piece outside the discharge zone, and the plasma jet outside the tube. The backward wave velocity exceeds essentially that of the forward wave. A reason is

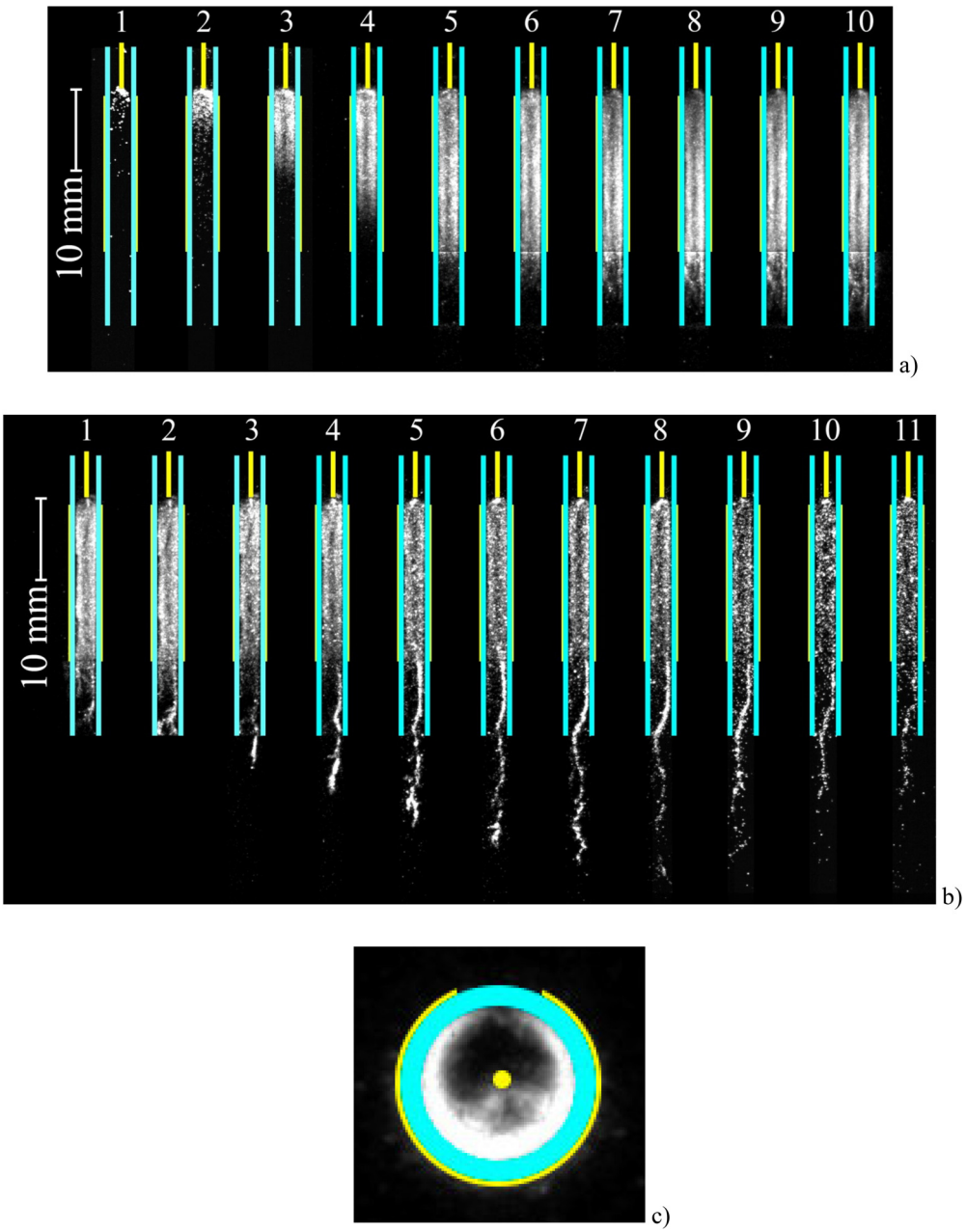

FIG. 5. A set of images (side view) of the discharge and plasma jet structures during the first breakdown development (a) and after the breakdown (b). The frame numbers in (a) and (b) correspond to the label numbers in Figs. 4(a) and 4(b). The exposure time of each frame is 51 ns. (c) The image of an almost azimuthally homogeneous tubular discharge structure inside the tube (view along the tube axis). The image corresponds to frame number 5 in (a).

that backward wave propagates along the plasma previously formed by the forward wave. One can see in Fig. 9 that the velocities of all ionization waves in the second half-cycle of the zug are less than those in the first half-cycle approximately by a factor of 10. As to subsequent half-cycles in the zug, all discharge structures listed above are repeated but with a gradual decrease in their severity due to the voltage amplitude attenuation (see Fig. 2).

B. Part II ($\tau < t_r$). The zug repetition frequency $F = 20$ kHz, $\tau = 50$ μs

As the zug repetition frequency F increases, the concentration of residual plasma from the previous zug increases. That leads to a decrease in both the breakdown voltage and its statistic scatter already in the first half-cycle of the every zug. This effect begins to manifest itself at the threshold frequency of $F = 1$ kHz, when $t_r \approx \tau$. At last, at

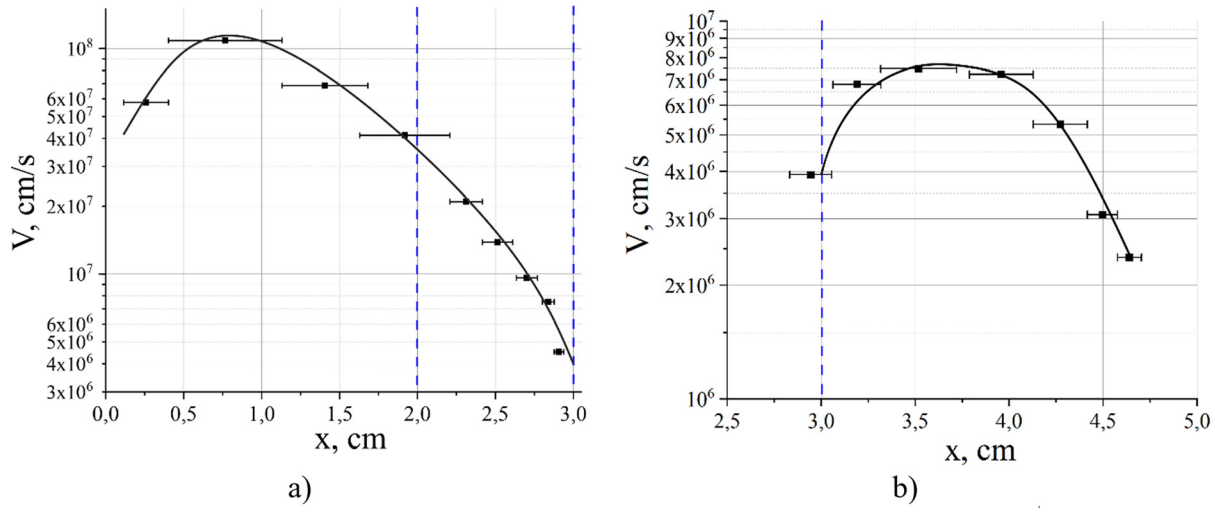

FIG. 6. (a) The propagation velocity of surface ionization waves in/out of the discharge zone. (b) The volume streamer propagation velocity outside the discharge tube. The vertical dotted blue lines show the boundaries of the discharge zone end (x = 2 cm) and the tube outlet (x = 3 cm).

frequency of $F = 20$ kHz, the breakdown voltage well stabilizes around the value of $U_b \approx 1.2 \pm 0.2$ kV, with good repeatability of the developing plasma structure in the course of several neighboring zugs. Therefore, the main results of Part II are given at a repetition rate of $F = 20$ kHz.

The characteristic voltage and current waveforms of a single zug as well as the amount of energy deposited in each half-cycle of the zug are shown in Fig. 10. Because the first breakdown voltage decreased, the amplitude of the pulse current of this breakdown decreased significantly. At the same time, an increase in the repetition frequency of the zugs did not significantly reduce the energy deposited in the discharge during one zug (275 μJ at $F = 20$ kHz vs 295 μJ at $F = 100$ Hz). The magnitude of energy deposition can be a useful information to find out the specific mechanism of ionization instability, developing of which leads to the diffuse tubular plasma constriction, that is, to the surface streamer formation.

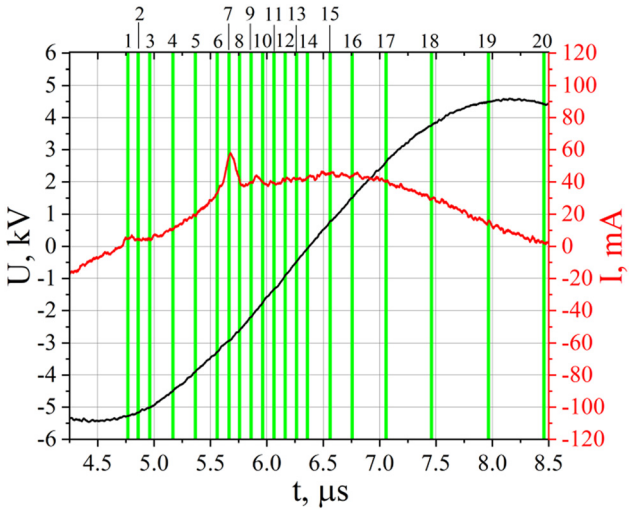

FIG. 7. The current and voltage waveforms at the voltage growth ($\partial U/\partial t > 0$) starting from the first negative half-cycle. The vertical green lines show the position on the time axis of the frames presented in Fig. 8. The label numbers of the lines correspond to the frame numbers in Fig. 8.

1. F = 20 kHz. Discharge structure in the first positive period at the stage $\partial U/\partial t > 0$

The current and voltage waveforms corresponding to the pointed conditions are presented in Fig. 11. This figure shows in close-up the clipping from the current waveform presented in Fig. 10. The clipping corresponds to the time interval around the breakdown and far after it. The vertical green lines show the position on the time axis of the frames presented in Fig. 12. The label numbers of green lines correspond to the frame numbers. Thus, electrical and optical information are well synchronized. The discharge current is positive till to 10th label number. According to Fig. 11, the breakdown dynamics is taken by frames 1–5 in Fig. 12.

In Fig. 12, the set of frames demonstrates the discharge and plasma jet structures' dynamics in the second positive half-cycle ($U > 0$) starting from the voltage $U \approx 0$ (see Fig. 10). Looking the frames 1–5, one can see the breakdown takes time about 0.5 μs and is accompanied by the surface tubular wave propagation toward the discharge exit. This process provides the increase in plasma conductivity in the discharge zone that eventually leads to the increase in potential at the tube exit. High potential initiates the volume streamer formation in the plasma jet. The last rapidly and rectilinearly propagated along the jet (frames 9–13).

We would like to attract the attention to the new phenomenon that appears only at high repetition frequency of the zugs. At this condition, a backward surface ionization wave arose being initiated by volume streamer. This wave has the form of a surface streamer that propagates along the inner tube surface from its exit into (!) the discharge zone (frames 12–15). Recall that at a frequency $F = 100$ Hz, the backward surface wave occurred before appearing the volume streamer

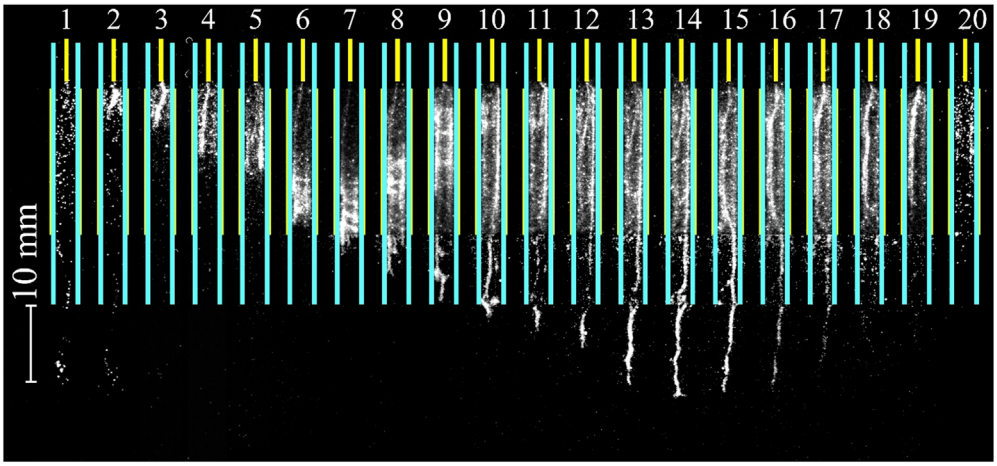

FIG. 8. A set of the discharge images in the first negative half-cycle under the growing voltage ($\partial U/\partial t > 0$, $I > 0$). The frame numbers correspond to the label numbers in Fig. 7. $F = 100$ Hz.

in the plasma jet, and it had a tubular but not surface streamer structure (Fig. 8). The new backward wave occurs at the stage of voltage and current diminishing, that is, at the decaying, a volume streamer is in a plasma jet. A volume streamer decays with a decrease in its luminosity and length. The streamer's length is shortened due to movement of its tail toward the tube exit. At the same time, the total visible length of the surface and volume streamers is preserved.

Information about the velocity distribution of the forward and backward surface ionization waves inside the tube as well as the streamer velocity in the plasma jet is shown in Fig. 13. Recall that the coordinates $0 \le x \le 2$, $2 \le x \le 3$, and $x > 3$ correspond to the discharge zone, the tube piece outside the discharge zone, and zone outside the tube, respectively. The coordinate $x = 0$ corresponds to a high-voltage electrode tip. The velocities of all ionization waves propagating both inside and outside the tube have a non-monotonic dependence on the x coordinate. One can emphasize that the tube outlet is an extremal boundary at which a surface streamer arriving with deceleration transforms into a volume streamer that propagates further with acceleration within the plasma jet.

A comparison of Figs. 13 and 9 reveals the main difference between the discharge mode with $F = 20$ kHz and the mode with $F = 100$ Hz under increasing the voltage $\partial U/\partial t > 0$. It consists in the fact that the maximum velocities of direct surface and volume ionization waves in the mode with $F = 20$ kHz are lower than those in the mode with $F = 100$ Hz.

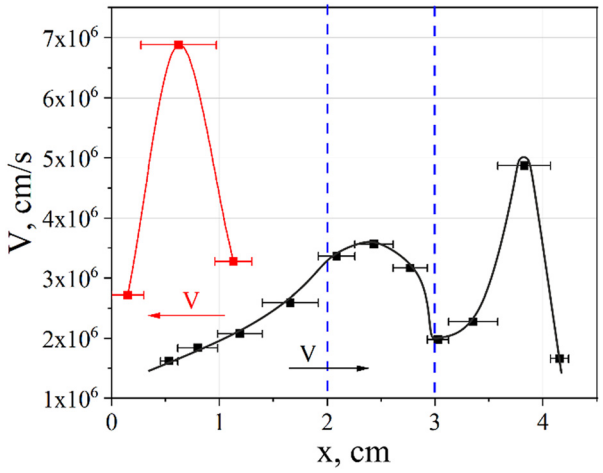

FIG. 9. The surface ionization waves velocity distribution in/out the tube. Experimental conditions are the same as in Fig. 8. Coordinate $x = 0$ corresponds to a high-voltage electrode tip. Dotted blue lines mark the discharge zone and tube outlet boundaries. The curves of black and red color correspond to the forward and backward wave, respectively.

2. F = 20 kHz. Breakdown and discharge structure at the stage $\partial U/\partial t < 0$

The further discharge evolution occurs at the voltage diminishing ($\partial U/\partial t < 0$, $I < 0$). The current and voltage waveforms corresponding to this regime are presented in Fig. 14.

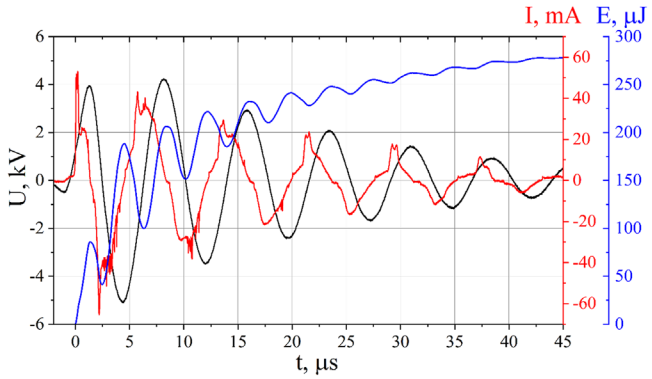

FIG. 10. The discharge voltage and current waveforms as well as the energy deposited into the discharge over the entire zug. $F = 20$ kHz.

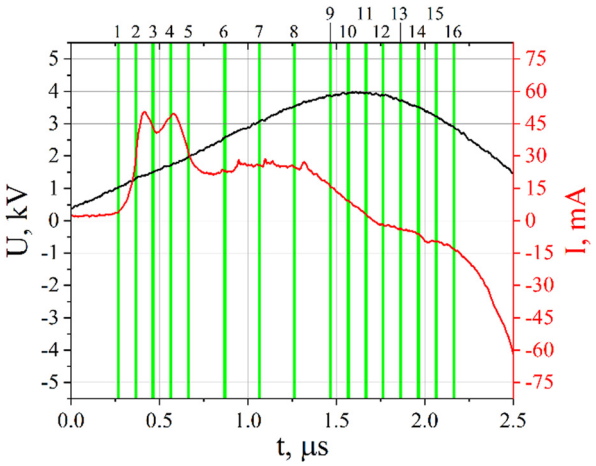

FIG. 11. The detail current and voltage waveforms at the second half-cycle with positive voltage starting from the voltage $U \approx 0$ (see Fig. 10). The label numbers of green lines correspond to the frame numbers in Fig. 12. $F = 20$ kHz.

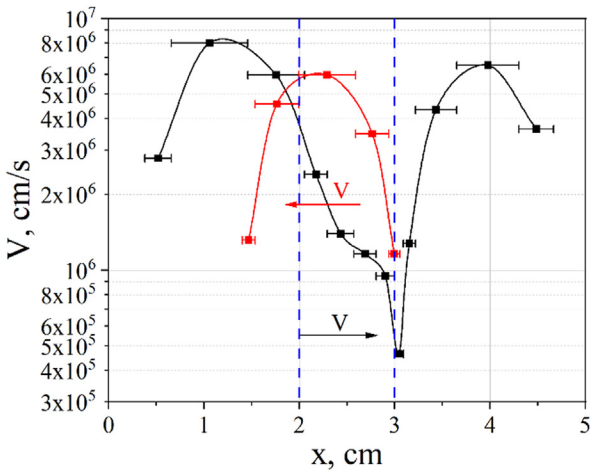

FIG. 13. The velocity distribution of surface ionization waves within the tube and volume streamer in the plasma jet. The black and red curves correspond to the forward and backward ionization waves, respectively. The vertical dotted blue lines mark the discharge zone and the tube outlet boundaries. $F = 20$ kHz.

The series of frames in Fig. 15 shows the dynamics of this evolution. At the beginning of the voltage drop, there is the decaying volume streamer created at the previous half-cycle (frame 1). At the same time, a new tubular ionization wave is formed at the high-voltage electrode and moves toward the discharge zone exit (Fig. 15, frames 2–6). This process is accompanied by an increase in the current (see Fig. 14), which reaches a maximum when the tubular wave arrives in the discharge zone exit (Fig. 15, frame 6).

Next, the current decreases and reaches a quasi-stationary level (Fig. 14). In this mode, a surface streamer forms outside the discharge zone and moves to the tube outlet and initiates here a volume streamer formation (Fig. 15, frame 7). Qualitative explanation of the surface streamer transformation into a volume streamer sounds as follows. To begin with, let us recall that the incipient stage of the volume streamer formation takes place in the vicinity of a sharpened needle tip stressed under high voltage. At this stage, the needed electric field strength providing the initial ionization avalanches development is created by the geometric effect, leading to strong focusing the electric field lines onto the tip. After streamer formation only, the space charge at the streamer head appears, which creates the needed electric field providing the volume streamer self-propagation.

Due to the surface streamer body high conductivity, such thin streamer can be considered, in a certain sense, as analogues of a needle connected with high-voltage electrode and able to stretch over the tube inner surface toward the tube exit. The sharpened needle tip transfers the potential of high-voltage electrode along the tube, and when it reaches the tube edge, the high potential appears at this place. At this moment, according to the earlier, a typical situation for the volume streamer initiation arises. The same event happens, when the head of a thin high conductive surface streamer reaches the tube exit. Based on the analogy earlier, we can say that the space charge of the surface

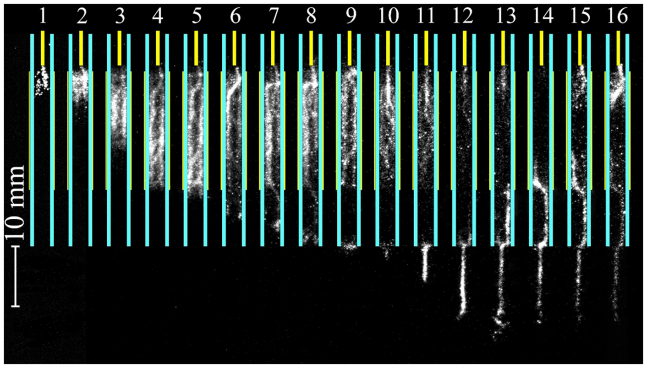

FIG. 12. The set of the consistent discharge and plasma jet images formed in the first half-cycle. The frame numbers correspond to the label numbers in Fig. 11. The exposure time of each frame is 100 ns. $F = 20$ kHz.

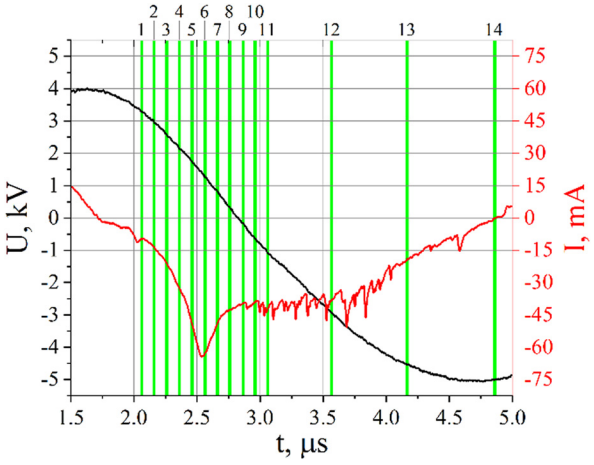

FIG. 14. The detail current and voltage waveforms at the regime with $\partial U/\partial t < 0$. The label numbers of green lines correspond to the frame numbers in Fig. 15. $F = 20$ kHz.

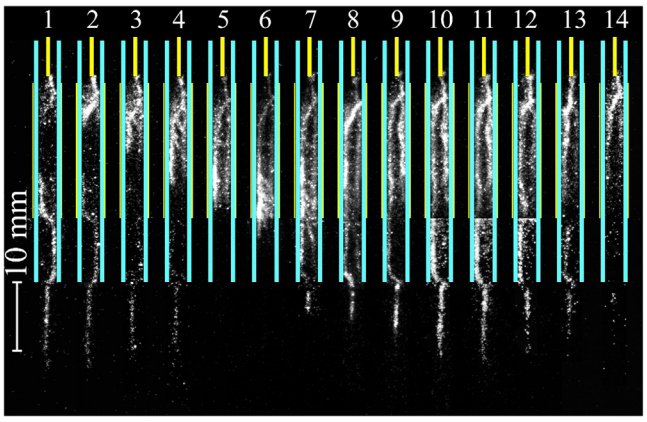

FIG. 15. The set of the discharge and plasma jet images corresponding to the regime with $\partial U/\partial t < 0$, $I < 0$. The frame numbers correspond to the label numbers in Fig. 14. The exposure time of the frames is 100 ns. F = 20 kHz.

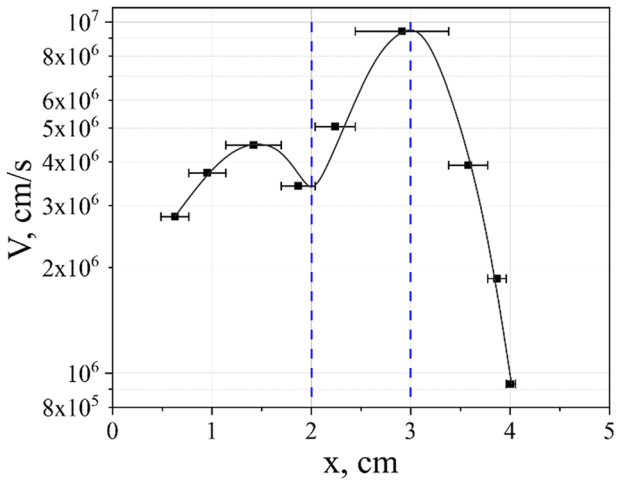

FIG. 16. The velocity distribution of surface ionization waves within the tube and volume streamer in the plasma jet. The discharge regime corresponds to condition $\partial U/\partial t < 0$, $I < 0$. The vertical dotted blue lines mark the discharge zone end and the tube outlet boundaries. $F = 20$ kHz.

streamer head has no crucial role in the volume streamer formation at the tube exit compared to the high electric potential or high electric field strength around the streamer head, created by streamer head at this place.

For the surface charge role, one can say the following. A surface streamer is actually the surface ionization wave charging the distributed capacity of a dielectric barrier along the streamer propagation trajectory. In a one-dimensional approximation, the propagation of this charging wave can be described by the linear diffusion equation of potential U, which has the form $\frac{\partial U}{\partial t} = D\frac{\partial^2 U}{\partial x^2}$.[25] The "diffusion" coefficient D is proportional to the plasma conductivity σ of the surface streamer and the barrier thickness δ but inversely to its dielectric constant ε: $D \sim \frac{\sigma\delta}{\varepsilon}$. From the diffusion coefficient definition, it follows the greater the streamer conductivity, the faster the high potential of the electrode reaches the tube edge. According to the diffusion equation, the value of the streamer local potential on the barrier is uniquely related to the local value of the surface charge deposited by streamer. Therefore, both statements "a high potential of the surface streamer head at the tube edge causes the volume streamer initiation," and "accumulation of a large surface charge by the surface streamer head at the tube edge causes the volume streamer initiation" are equivalent to each other.

The volume streamer spreads along the jet and, having reached its maximum length, gradually decays. In this case, the plasma structure inside the tube also disappears (Fig. 15, frames 7–14).

The velocity distribution of surface ionization waves within the tube and volume streamer in the plasma jet for the discharge regime with $\partial U/\partial t < 0$ is pictured in Fig. 16. The velocities of all ionization waves have a non-monotonic dependence on the x coordinate.

To the following periods of the zug, the described structures are repeated, but with a gradual decrease in their severity, until they completely disappear when the discharge current stops.

C. Lifetime of surface plasma structures in a tube

The surface streamer created every half-cycle leaves a trace during its propagation. This trace is formed by a deposited surface charge and near-surface plasma. The presence of such trace promotes the propagation of new surface streamer in the next half-cycle closely following the trajectory of the former streamer. In this case, the question arises: how long can a once-created pattern of surface plasma structure be repeated in a periodic discharge? Theoretically, it is very difficult to estimate the "lifetime" of an arbitrary plasma pattern. Therefore, its experimental determination is of interest. In the experiment, this lifetime was identified with the time within which the image of an arbitrary plasma pattern more or less saves its shape. For this purpose, the discharge images were taken with different delay between frames both within the same zug and between neighbor zugs. The results are shown in Figs. 17 and 18.

Figure 17 demonstrates a good reproducibility of an arbitrary plasma structure in the tube during the entire zug at low and high frequency of its repetition F = 100 Hz and 20 kHz. This fact means the lifetime of the surface plasma pattern exceeds the duration of the zug equal to 45 μs.

Figure 18 shows the discharge plasma structures in several consecutive zugs at their repetition frequencies of F = 1 and 20 kHz. The current and voltage waveforms for these zugs are given in Figs. 18(a) and 18(b). Figure 18(c) demonstrates the absence of similarity of plasma structure patterns at F = 1 kHz. This means that the lifetime of plasma structure patterns is less than 1 ms. Figure 18(d) presents the set of the discharge images at F = 20 kHz. One can see that the images of three consecutive zugs (frames 1–3) show an approximate similarity of plasma structure patterns, which persists for no more than 100 μs.

D. Plasma jet structure

The plasma jet structure is formed not only by brightly luminous volume streamers but also by weakly luminous diffuse plasma. To demonstrate this fact more clearly, images of the plasma jet were obtained at different zug repetition frequencies and at long exposure time. It allowed one to detect the faint diffuse plasma surrounding the bright volume streamer. The results are presented in Fig. 19 for low and high zug repetition frequency.

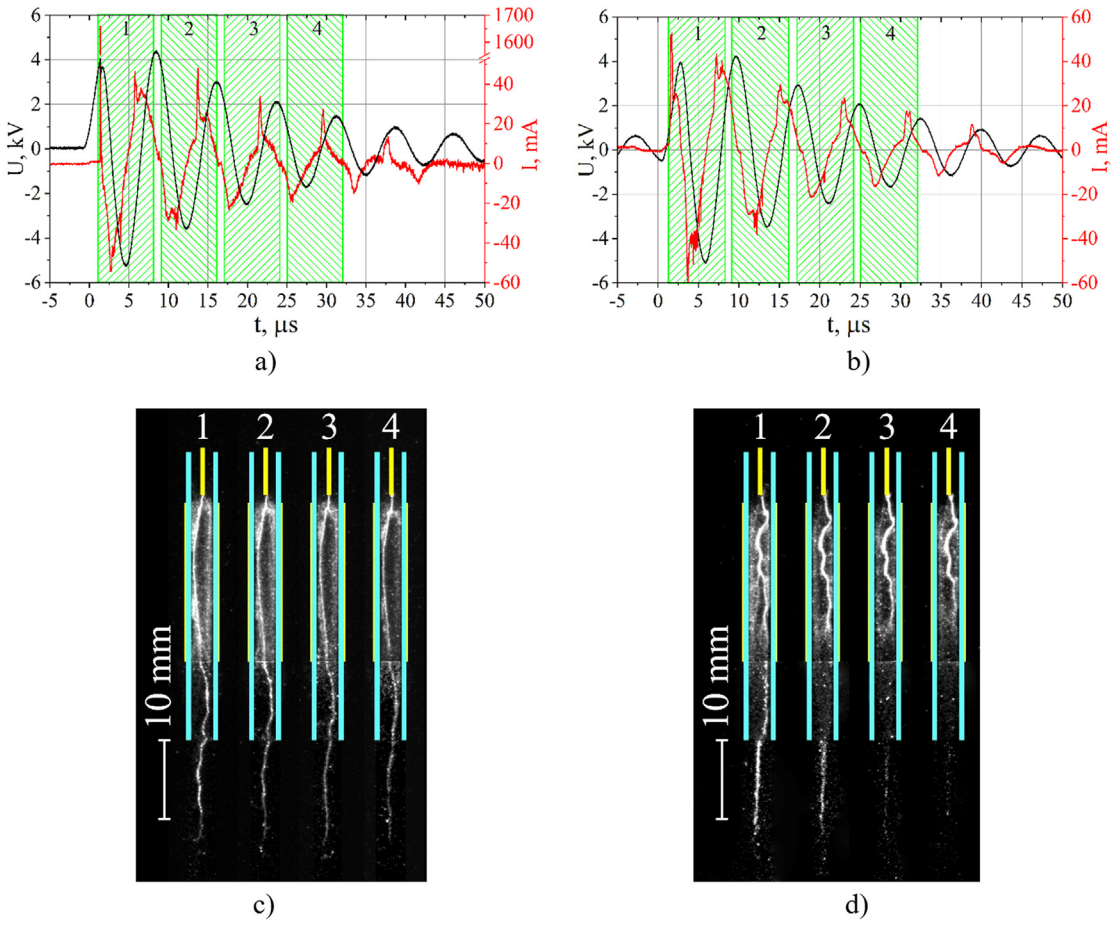

FIG. 17. The voltage and current waveforms of zugs with different repetition frequencies: (a) $F = 100$ Hz and (b) $F = 20$ kHz. The vertical labels with numbers correspond to the time points, at which the frames in (c) and (d) were taken. The plasma structures images taken in four consecutive periods in zug: (c) $F = 100$ Hz and (d) $F = 20$ kHz. The exposure time of each frame is 7 μs.

Figure 19(a) corresponds to low repetition frequency F = 100 Hz and demonstrates a bundle of the volume streamers flowing down from the tube inner surface and forming a plasma jet. This image is an artificial photography, which was obtained by superimposing images of 10 single streamers taken from 10 randomly selected zugs. One can see that every volume streamer starts from a random location on the inner surface of the tube exit and moves in the jet along a curved snake-like trajectory or, more likely, along a helical line. The place of the streamer starting from the tube is chaotically and quickly changing in time. Just this circumstance leads to an illusion about axial symmetry of the plasma jet seeing with the naked eye. Dim diffuse plasma around streamer is invisible with an exposure time of 45 μs.

Figures 19(b) and 19(c) present the plasma jet views formed by superimposing the images of jets being creating by six consecutive zugs. F = 600 Hz; exposure time 240 μs (six consecutive zugs). In this case, axisymmetric cone of diffuse plasma is visible around the curved volume streamers. Thus, the bright streamer moves along the jet surrounded by dim diffuse plasma. At the tube outlet, the diffuse plasma cross section is equal to the tube inner cross section.

As the zug repetition frequency increases [Fig. 19(d), F = 20 kHz], the volume streamer moves along an increasingly rectilinear trajectory along the jet axis.

E. Simultaneous image of all plasma structures of the coaxial barrier discharge

A clear difference in plasma structures in the three regions of the barrier discharge—in the tube within the discharge zone, in the tube outside the discharge zone, and in the plasma jet outside the tube—is shown in Fig. 20 at F = 100 Hz. The picture is an integral image of the discharge and plasma jet formed by one zug, that is, this image is an overlay of images of the discharge and jet from all half-periods of one zug. At the short exposure time, the weak diffuse glow of the plasma jet is not detected. The photos were taken with a Canon EOS 5D camera. The comments to Fig. 20 are the following. Inside the tube, the main surface streamer is visible, continuous along the entire length of the tube and transforming into a volume streamer at the outlet. Short transverse streamers are visible in the discharge zone, collecting current into the main streamer.

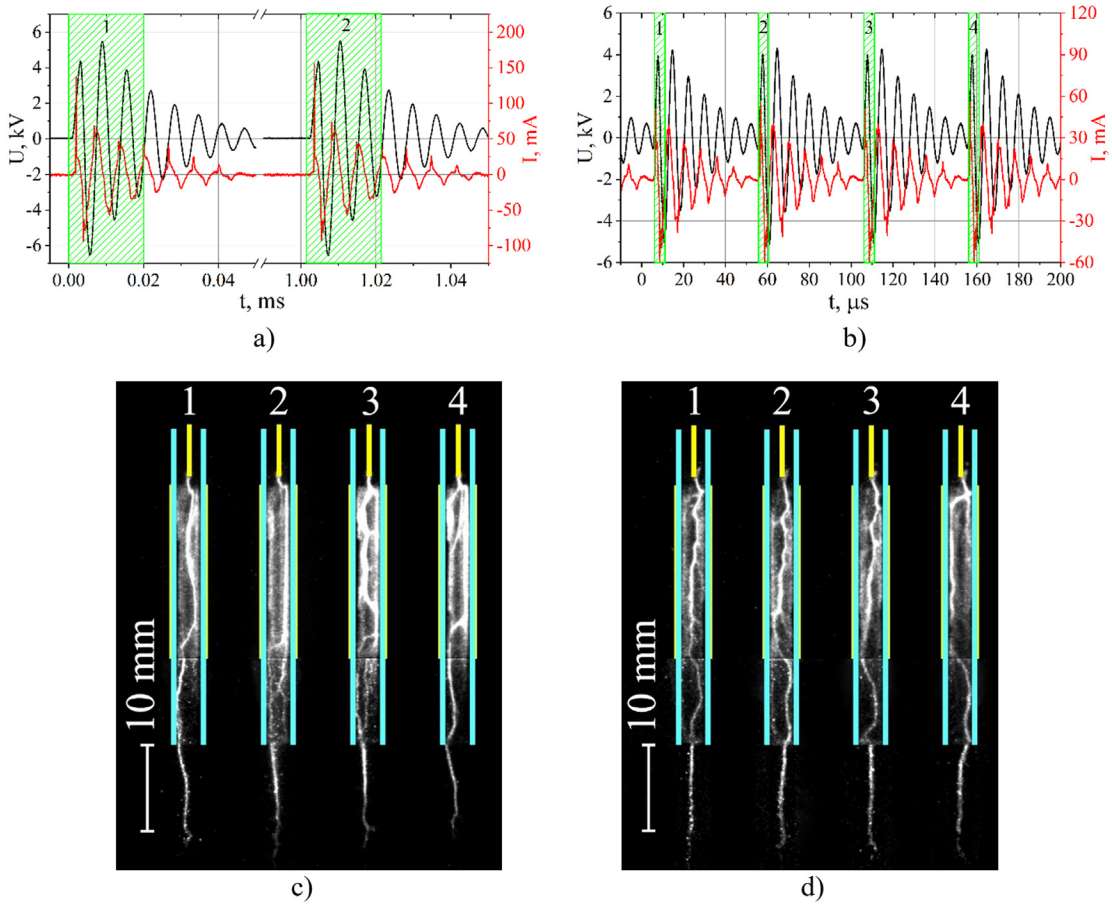

FIG. 18. Voltage and current waveforms of the zugs: (a) $F = 1$ kHz and (b) $F = 20$ kHz. The vertical green labels 1–2 (a) and 1–4 (b) correspond to the time points at which the frames in figures (c) and (d) were taken. (c) $F = 1$ kHz; the exposure time is 20 μs. (d) $F = 20$ kHz; the exposure time is 5 μs.

IV. DISCUSSION

A. Discharge zone

If the tubular geometry of the coaxial barrier discharges to unfold in a plane, the surface barrier discharge of the plane geometry will be obtained. It follows that these discharges are of the same type in terms of current generation mechanisms in them. In this case, parallels can be drawn between the plasma structures of both discharges. For example, in Ref. 25, devoted to the study of a streamer surface barrier discharge in a pin-plane geometry, it was shown that numerous small streamers branch off from the main surface streamer, in order to supply current to it. In addition, both the main surface streamer and the small streamers are surrounded by faintly luminous diffuse near-surface plasma, which also supplies current to the constricted structures (Fig. 21).

The plane barrier discharge is essentially a plasma capacitor with variable capacitance. In such a case, the discharge current $I = C\frac{\partial U}{\partial t} + U\frac{\partial C}{\partial t}$ is determined by the time behavior of the applied voltage $U(t)$ and capacitance $C(t)$ created by near-surface plasma sheet.[25] The latter value is proportional to the instantaneous area of the entire plasma structure in contact with the dielectric barrier. The contact area of the constricted structure (thin surface streamers) is small, but the current carried in these streamers is large. To overcome this contradiction and provide the necessary current into the streamers, diffuse plasma appears around them over a large area. For exactly the same reason, there are simultaneously both the constricted and diffuse plasma structures on the tube inner surface in a coaxial barrier discharge.

Differences in the first breakdown voltage amplitude at $F = 100$ Hz and $F = 20$ kHz ($U_b = 4$ and 1.3 kV) lead to a difference in plasma structures formed in the discharge zone. With a low repetition frequency, in the discharge zone, there is a main surface streamer extending over the entire length of this zone [Fig. 20(a)]. There are also transverse short surface streamers collecting current into the main streamer from the tubular surface plasma sheet. Such structure is similar to that in a flat barrier discharge in the streamer mode.

When looking at Fig. 20, one may get the wrong impression that the main streamer is a volume streamer extending approximately along the axis of the discharge tube. In fact, one need to take into account the presence of a slit on the external electrode. Calculations show that the maximum electric field strength inside the tube occurs on the surface area at maximum distance from the slit. This is why the

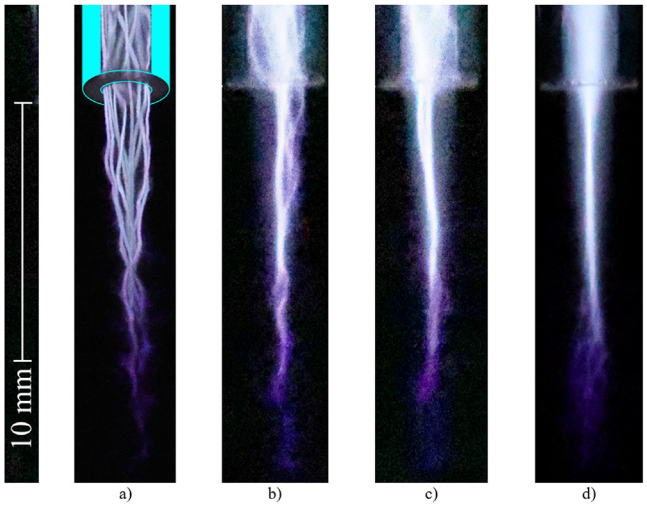

FIG. 19. (a) An artificial image of a bundle of 10 streamers flowing down from the tube inner surface and forming a plasma jet. $F = 100$ Hz, exposure time 45 μs. (b) and (c) The plasma jet image formed by superimposing jet images of six consecutive zugs. $F = 600$ Hz; the exposure time is 240 μs (six consecutive zugs). (d) A view of axisymmetric cone of diffuse plasma and a bright axisymmetric channel formed by superimposing images of all streamers from 100 consecutive zugs. $F = 20$ kHz; the exposure time is 0.5 ms (100 zugs).

plasma in the tube forms more intensively in this area, and the surface wave takes on the shape of a crescent [Fig. 5(c)]. Just in this area, ionization instability will develop most quickly, and a surface streamer will form here. Photographing was performed in the direction of the surface area indicated above. If the camera depth of field is greater than the inner diameter of the tube, a false impression arises that the surface streamer is the volume one.

As it turned out, the maximum velocities of surface ionization waves inside the tube at high repetition frequency of F = 20 kHz are much lower than the velocities of ionization waves at low frequencies of F = 100 Hz. The reason is that the voltage of the first breakdown, on which the velocities of the ionization waves depend, is lower at high repetition frequency than that at low frequency. The low breakdown voltage at a high repetition frequency is explained by the fact that the concentration of residual plasma from the previous zug is sufficient to promote the breakdown in the subsequent zug.

B. Plasma jet

The intensity of the plasma jet glow is determined by the collective radiation of a bright volume streamer and the dim diffuse plasma surrounding it. Photographing plasma jets showed the dependence of

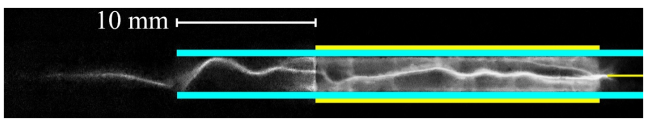

FIG. 20. Integral image of the plasma structure inside the tube and in the plasma jet. The weak diffuse glow of the plasma jet is not detected. The exposure time of 45 μs is equal to the duration of one zug. Gas flow direction is from right to left. $U_b = 4$ kV. $F = 100$ Hz.

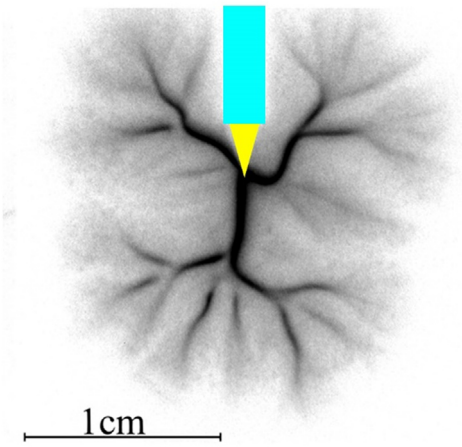

FIG. 21. The image of plasma structure of a pulsed surface barrier discharge in the pin-to-plane geometry (top view). $P = 1$ atm. Reproduced with permission from Akishev *et al.*, Plasma Sources Sci. Technol. **22**, 015004 (2012). Copyright 2012 IOP Publishing.[25] The blue color is a dielectric tube; the yellow color is a pointed metal pin with a diameter of 1 mm inserted tightly into the tube.

the streamer trajectory shape on the repetition frequency of the zugs. At a low frequency of F = 100 Hz, the volume streamer propagates along a curved trajectory, more like a helical line with a decreasing diameter. At a high frequency F = 20 kHz, it propagates in a straight line and strictly along the jet axis. This result is consistent with the results of Ref. 20, which observed the rectilinear propagation of a streamer in a jet formed by a microwave discharge.

The surface streamer behavior has a weak dependence on the zug frequency. However, the shape of the volume streamer trajectory depends on the zug frequency. Possibly, the difference in the trajectories shape of volume streamers can be connected with difference of the medium, through which the very first streamers in every zug propagate. Indeed, at F = 100 Hz, the plasma created in jet by streamers of previous zug will be full removed by gas flow to the beginning of subsequent zug. Thus, the first streamer will propagate along argon jet through non-preionized gas. The next streamers in the zug will propagate along the trajectory created by the first streamer. At F = 20 kHz, all streamers propagate through the jet filled with plasma. At present, the mechanism leading to the curvature of the volume streamer trajectory at F = 100 Hz is unknown.

For most part of the visible length of the volume streamer, it does not change its transverse size. The streamer characteristic diameter increases with an increase in the repetition frequency of the zugs. So, at F = 100 Hz, the diameter d = 0.3 ± 0.05 mm, and at F = 20 kHz, the diameter d = 0.55 ± 0.05 mm. One of the possible reasons of the streamer diameter increasing is the gas heating in the jet, which is more intensive at higher repetition frequency. The maximum velocity of a rectilinear streamer in a jet at F = 20 kHz is close to the velocity of a curved streamer at F = 100 Hz. A reason for that is not clear and requires additional study.

The plasma jets images (Fig. 19) show a large spatial amplitude of chaotic transverse oscillations of the streamer's tail. A possible reason for these oscillations can be the following. At the beginning, volume streamer propagates at a velocity exceeding that of the gas jet.

Furthermore, the streamer slows down at the end of its journey and reduces the velocity down to the speed of a turbulent flow. In such a case, trajectory of slow streamer's tail can easily be influenced by turbulent pulsations of the gas flow.

The dim diffuse plasma in the jet plays an important role in the propagation of a fast volume streamer, as it supplies seed electrons to the streamer front. Therefore, there is no need to attract a gas photoionization to explain the positive volume streamer propagation in a plasma jet. This conclusion is also true for a negative volume streamer generated by a negative voltage pulse. Although it should note that the negative volume streamer is able itself to supply the front with seed electrons due to their transportation from its body, in such a case, it is quite possible that negative volume streamer could be less sensitive to the external plasma existence compared to the positive volume streamer.

However, the mechanism of formation and maintenance of a dim diffuse plasma in the jet has not yet been established. Three hypotheses can be put forward: (a) diffuse plasma is blown out of the tube and moves with gas at a flow velocity; (b) diffuse plasma is rapidly created when the ionization front of the volume streamer propagates; (c) diffuse plasma is relatively slowly created by the radial electric field around of the streamer body. This E-field will diminish along the streamer, which should lead to decreasing the diffuse plasma radius as the streamer length increases. However, all these hypotheses require further study.

It can be added that the radial profile of the diffuse plasma glow can also be affected by the ambient air flowing into the jet. On the one hand, the air quenches the radiating and metastable states of argon and, on the other hand, intensively converts the electrons of the diffuse plasma into negative ions, which quickly recombine with positive argon ions. This effect also requires special research.

C. The lifetime of plasma structures

It follows from the results shown in Figs. 17 and 18 that the typical lifetime of plasma structures in a coaxial barrier discharge tube in argon flow at atmospheric pressure is about 100 μs. During this time, the plasma density in the constricted structures decreases due to recombination to about $10^{11}\,\mathrm{cm}^{-3}$. It turns out that the residual plasma density below $10^{11}\,\mathrm{cm}^{-3}$ is sufficient to reduce the breakdown voltage at the HV tip but not enough to ensure the formation of a new plasma structure in the trace of the previous structure.

V. CONCLUSION

In this work, devoted to a coaxial barrier discharge in argon flow, the complex plasma structure inside a gas-discharge tube and in plasma jet is clarified. This structure is non-stationary and does not repeat itself at times greater than the time of gas passage through the tube. The dynamics of the spatial structure inside a discharge tube is determined mainly by surface ionization waves, which can be divided into azimuthally homogeneous (tubular ionization wave) and constricted (surface streamers) waves. In turn, the structure of surface streamers consists of the main streamer body, and many short side streamers look like branches growing from the main body. The discharge current is ensured by the propagation of the total plasma structure along the tube. The transition of surface waves through the boundaries at the outlets of both the discharge zone and the quartz tube is accompanied by a change in their velocity. The maintenance of a high current density in the main streamer body is provided in large part by the current from an azimuthally homogeneous surface wave. In addition, the current collection into main body happens through numerous thin side short streamers.

The plasma jet structure is also non-stationary and formed by propagation of both brightly glowing thin volume streamers and a wide faintly luminous diffuse plasma. Streamers propagate along the jet at a speed exceeding the convective velocity of gas flow. At $F = 100\,\mathrm{Hz}$, streamers move in a jet along a curved snake-like trajectory or, more likely, along a helical line. The question of the exact shape of the streamer trajectory in the jet and the mechanism creating the curved trajectory remains open now. At $F = 20\,\mathrm{kHz}$, streamers propagate in the jet in a straight line along its axis. At all frequencies, the streamers slow down to the velocity of a turbulent gas flow at the end of their journey. Perhaps, at low velocity, streamers begin to noticeably react to the turbulent fluctuations of gas flow, which leads to strong chaotic displacements of the streamer's tail in the transverse direction.

In conclusion, numerical modeling plays an important role in determining the composition and concentration of reactive particles produced by a coaxial barrier discharge. To be adequate, the mathematical model should describe the plasma structure in the tube and in the jet as a single object combined by ionization and gasdynamic processes. In this case, it is necessary to have experimental information about the real dynamic structure of the discharge inside the tube and in the plasma jet. Knowledge of the real structure will make it possible to create simplified mathematical models that, nevertheless, capture the main features of gas-discharge and plasma-chemical processes. Thus, the earlier justifies the scientific significance of the results obtained in this work.

ACKNOWLEDGMENTS

This work was carried out within the framework of the Russia–Iran joint project and was supported by the Russian Science Foundation (Grant No. 24-45-20006) and the Iranian National Science Foundation (Grant No. 4023625).

AUTHOR DECLARATIONS

Conflict of Interest

The authors have no conflicts to disclose.

Author Contributions

Yu. Akishev: Conceptualization (lead); Supervision (lead); Writing – original draft (lead); Writing – review & editing (lead). **S. Ermolaeva:** Funding acquisition (lead); Project administration (lead); Supervision (supporting). **M. Medvedev:** Data curation (equal); Investigation (equal); Visualization (equal). **A. Petryakov:** Data curation (equal); Investigation (lead); Visualization (equal). **K. Hajisharifi:** Data curation (equal); Formal analysis (equal); Software (equal). **H. Mehdian:** Conceptualization (equal); Methodology (equal). **E. Robert:** Methodology (equal); Software (equal).

DATA AVAILABILITY

The data that support the findings of this study are available within the article.

REFERENCES

[1]A. Bogaerts, E. Neyts, R. Gijbels, and J. van der Mullen, "Gas discharge plasmas and their applications," Spectrochim. Acta, Part B **57**, 609–658 (2002).

[2]R. Brandenburg, K. H. Becker, and K.-D. Weltmann, "Barrier discharges in science and technology since 2003: A tribute and update," Plasma Chem. Plasma Process. **43**, 1303 (2023).

[3]M. Keidar, K.-D. Weltmann, and S. Macheret, "Fundamentals and applications of atmospheric pressure plasmas," J. Appl. Phys. **130**, 080401 (2021).

[4]*Plasma Applications in Gases, Liquids and Solids: Technology and Methods*, edited by C. Riccardi and H. Eduardo Roman (World Scientific, 2023), p. 296.

[5]K. D. Weltmann, E. Kindel, T. von Woedtke, M. Hähnel, M. Stieber, and R. Brandenburg, "Atmospheric-pressure plasma sources: Prospective tools for plasma medicine," Pure Appl. Chem. **82**(6), 1223–1237 (2010).

[6]X. P. Lu, S. Reuter, M. Laroussi, and D. W. Liu, *Nonequilibrium Atmospheric Pressure Plasma Jets: Fundamentals, Diagnostics, and Medical Applications* (CRC Press, Boca Raton, FL, 2019).

[7]R. K. Chailakhyan, A. G. Grosheva, Y. V. Gerasimov, N. N. Vorob'eva, S. A. Ermolaeva, E. V. Sysolyatina, A. V. Petryakov, and Y. S. Akishev, "Effect of non-thermal plasma on proliferative activity and adhesion of multipotent stromal cells to scaffolds developed for tissue-engineered constructs," Bull. Exp. Biol. Med. **167**, 182–188 (2019).

[8]T. von Woedtke, S. Emmert, H.-R. Metelmann, S. Rupf, and K.-D. Weltmann, "Perspectives on cold atmospheric plasma (CAP) applications in medicine," Phys. Plasmas **27**, 070601 (2020).

[9]M. Laroussi, S. Bekeschus, M. Keidar, A. Bogaerts, A. Fridman, X. Lu, K. Ostrikov, M. Hori, K. Stapelmann, V. Miller *et al.*, "Low-temperature plasma for biology, hygiene, and medicine: Perspective and roadmap," IEEE Trans. Radiat. Plasma Med. Sci. **6**, 127–157 (2022).

[10]Y. Akishev, A. Balakirev, M. Grushin, V. Karalnik, I. Kochetov, A. Napartovich, A. Petryakov, and N. Trushkin, "Long plasma jet generated by DC discharge in N_2 at atmospheric pressure: Impact of trace admixtures on composition of reactive species in far afterglow," IEEE Trans. Plasma Sci. **43**(3), 745–752 (2015).

[11]A. Schmidt-Bleker, S. A. Norberg, J. Winter, E. Johnsen, S. Reuter, K. D. Weltmann, and M. J. Kushner, "Propagation mechanisms of guided streamers in plasma jets: The influence of electronegativity of the surrounding gas," Plasma Sources Sci. Technol. **24**(3), 035022 (2015).

[12]Y. Suenaga, T. Takamatsu, T. Aizawa, S. Moriya, Y. Matsumura, A. Iwasawa, and A. Okino, "Influence of controlling plasma gas species and temperature on reactive species and bactericidal effect of the plasma," Appl. Sci. **11**, 11674 (2021).

[13]Y. Akishev, G. Aponin, A. Petryakov, and N. Trushkin, "On the composition of reactive species in air plasma jets and their influence on the adhesion of polyurethane foam to low-pressure polyethylene," J. Phys. D: Appl. Phys. **51**, 274006 (2018).

[14]M. Teschke, J. Kedzierski, E. G. Finantu-Dinu, D. Korzec, and J. Engemann, "High-speed photographs of a dielectric barrier atmospheric pressure plasma jets," IEEE Trans. Plasma Sci. **33**, 310–311 (2005).

[15]Z. Chang, N. Zhao, G. Li, and G. Zhang, "Plasma 'bullet' with hollow structure: Formation and evolution," Sci. Rep. **8**, 7599 (2018).

[16]A. Bogaerts and R. Gijbels, "Modeling of metastable argon atoms in a direct-current glow discharge," Phys. Rev. A **52**, 3743–3751 (1995).

[17]A. Bogaerts, R. Gijbels, and J. Vlcek, "Collisional-radiative model for an argon glow discharge," J. Appl. Phys. **84**, 121–136 (1998).

[18]P. Li, Z. Chen, H. Mu, G. Xu, C. Yao, A. Sun, Y. Zhou, and G. Zhang, "Confluence or independence of microwave plasma bullets in atmospheric argon plasma jet plumes," J. Appl. Phys. **123**, 123302 (2018).

[19]S. Reuter, J. Winter, S. Iseni, S. Peters, A. Schmidt-Bleker, M. Dünnbier, J. Schäfer, R. Foest, and K.-D. Weltmann, "Detection of ozone in a MHz argon plasma bullet jet," Plasma Sources Sci. Technol. **21**, 034015 (2012).

[20]Z. Chen, G. Xia, C. Zou, X. Liu, D. Feng, P. Li, Y. Hu, O. Stepanova, and A. A. Kudryavtsev, "Bullet-shaped ionization front of plasma jet plumes driven by microwave pulses at atmospheric gas pressure," J. Appl. Phys. **122**, 093301 (2017).

[21]S. Wu, Z. Wang, Q. Huang, X. Tan, X. Lu, and K. Ostrikov, "Atmospheric-pressure plasma jets: Effect of gas flow, active species, and snake-like bullet propagation," Phys. Plasmas **20**, 023503 (2013).

[22]J. J. Thomson, *Researches in Electricity and Magnetism* (Clarendon, Oxford, 1893), p. 115.

[23]Y. Akishev, T. Alekseeva, V. Karalnik, and A. Petryakov, "On the slow ionization waves forming the breakdown in a long capillary tube with helium at low pressure," J. Phys. D: Appl. Phys. **55**, 145202 (2022).

[24]L. M. Vasilyak, S. V. Kostyuchenko, N. N. Kudryavtsev, and I. V. Filyugin, Phys.–Usp. **37**(3), 247–269 (1994).

[25]Y. Akishev, G. Aponin, A. Balakirev, M. Grushin, V. Karalnik, A. Petryakov, and N. Trushkin, "Spatial–temporal development of a plasma sheet in a surface dielectric barrier discharge powered by a step voltage of moderate duration," Plasma Sources Sci. Technol. **22**, 015004 (2012).